01 Jan 2002

Hydrothermal Deposition and Characterization of Heteroepitaxial $BaTiO_3$ Films on $SrTiO_3$ and $LaAlO_3$ Single Crystals

Emin Ciftci

M. N. Rahaman
Missouri University of Science and Technology, rahaman@mst.edu

Frank D. Blum
Missouri University of Science and Technology

Recommended Citation

E. Ciftci et al., "Hydrothermal Deposition and Characterization of Heteroepitaxial $BaTiO_3$ Films on $SrTiO_3$ and $LaAlO_3$ Single Crystals," *Journal of Materials Science*, Springer-Verlag, Jan 2002.
The definitive version is available at https://doi.org/10.1023/A:1016593007572

JOURNAL OF MATERIALS SCIENCE **37** (2002) 3361 – 3367

Hydrothermal deposition and characterization of heteroepitaxial $BaTiO_3$ films on $SrTiO_3$ and $LaAlO_3$ single crystals

E. CIFTCI*, M. N. RAHAMAN*, F. D. BLUM‡
*Departments of *Ceramic Engineering and ‡Chemistry, University of Missouri, Rolla, Missouri 65409, USA*
E-mail: rahaman@umr.edu

Heteroepitaxial $BaTiO_3$ thin films were deposited in an aqueous solution under hydrothermal conditions on single crystal substrates of (100) $SrTiO_3$ and (012) $LaAlO_3$. The reactants consisted of fine TiO_2 particles in a strongly alkaline solution of $Ba(OH)_2$ at a temperature of 150°C. The growth of the films was studied by atomic force microscopy, high resolution scanning electron microscopy, and X-ray diffraction. The formation of the films occurred by nucleation of {001} faceted islands followed by three-dimensional growth of the islands to cover the substrate. Repeated hydrothermal treatment improved the film thickness and the surface coverage of the substrate at the expense of increased surface roughness. X-ray diffraction coupled with pole figure analysis showed that the films had the same in-plane and out-of-plane orientation as the substrate.

1. Introduction

Thin films of oxides with high dielectric constant are of significant interest for a variety of technological applications, such as dynamic random access memory (DRAM), sensors, thermistors and electroluminescent elements [1]. In addition, epitaxial growth of the films can be used to optimize the anisotropic properties of electronically important oxides such as barium titanate, $BaTiO_3$, and lead zirconate titanate, $Pb(Zr_xTi_{1-x})O_3$ (PZT). Conventional routes to the synthesis of ceramic thin films, such as sol-gel processing [2] and metal-organic chemical vapor deposition [3], require relatively high temperatures at which interdiffusion, interfacial reaction and evaporation of volatile constituents can lead to a deterioration of the electronic properties. There is interest in the electrochemical route [4–6], the hydrothermal route [7] or a combination of hydrothermal and electrochemical techniques [8, 9] for the synthesis of ceramic films from aqueous solutions because they can provide low temperature, alternative routes to the high temperature methods.

The growth of epitaxial films by hydrothermal deposition from aqueous solutions has been reported for simple oxides such as TiO_2 [10] and ZnO [11]. The hydrothermal route has been used to deposit $BaTiO_3$ films on titanium and silicon substrates [12–14]. Epitaxial $BaTiO_3$ and PZT films have also been deposited hydrothermally on $SrTiO_3$ single crystal substrates [15–19]. However, the parameters that control the epitaxial deposition and the mechanism of nucleation and growth are not clear.

The purpose of the work described here was to investigate the influence of key processing parameters on the nucleation and growth of $BaTiO_3$ films on single crystal substrates by deposition from aqueous solution under hydrothermal conditions. Films were deposited on (001) $SrTiO_3$ and (012) $LaAlO_3$ single crystals by reacting fine TiO_2 powder and a strongly alkaline solution of $Ba(OH)_2$ solution at 150°C in a Teflon-lined autoclave. The growth of the films was characterized by atomic force microscopy (AFM), X-ray diffraction (XRD) and scanning electron microscopy (SEM).

2. Experimental

The chemicals for the deposition of the $BaTiO_3$ films consisted of barium hydroxide octahydrate ($Ba(OH)_2 \cdot 8H_2O$; Aldrich, Milwaukee, WI) and TiO_2 (average particle size ≈25 nm; ~30 weight percent (wt%) rutile and ~70 wt% anatase; Degussa Corp., South Planefield, NJ). Four grams of $Ba(OH)_2 \cdot 8H_2O$ was added to 24 ml of deionized water in a Teflon-lined autoclave (45 ml capacity, Parr Instrument Co., Moline, IL). The system was purged with argon, sealed and heated for 3 h at 90°C to dissolve the $Ba(OH)_2 \cdot 8H_2O$ completely. One gram of TiO_2 powder was added to the solution (pH 13.3) and a polished single crystal of $SrTiO_3$ or $LaAlO_3$ (6.25 mm by 6.25 mm by 0.5 mm thick; Superconductive Components, Inc., Columbus, OH) was suspended in the solution using a Teflon thread. The autoclave was sealed and the system was heated to the reaction temperature (150°C) in 10 min.

This reaction temperature was chosen on the basis of earlier experiments on the synthesis of $BaTiO_3$ powders by the same reaction [20]. Two different deposition procedures were employed. In one case, the single crystal was held in the reactant solution for a given time and a different crystal was used in each run. In the second case, to investigate the nucleation and growth process progressively, the same crystal was used for repeated deposition steps. After each deposition step, the reactant solution in the autoclave was replaced with a fresh solution. Prior to characterization, the single crystals were washed with deionized water in an ultrasonic bath to remove loose particles from the surface of the film and dried at ∼80°C.

The crystalline structure of the deposited films was determined by XRD (XDS 2000; Scintag Inc., Sunnyvale, CA) using nickel filtered Cu K_α radiation ($\lambda = 0.15405$ nm) in a step-scan mode with $2\theta = 0.01^\circ$ per step. Texture analysis by XRD (pole figure analysis) was performed using a texture goniometer in which the crystal was tilted at a fixed 2θ angle (45°) corresponding to the angle between the {100} and {110} family of planes in the cubic structure, and rotated azimuthally. X-ray rocking curves were used to assess the crystalline quality of the film by comparing the width of the curve with its theoretical width. Rocking curves were acquired for the (100) reflections from the film and from the corresponding substrate.

Atomic force microscopy (Nanoscope III, Digital Instruments Inc., Santa Barbara, CA) was used to determine the crystal size, thickness and surface roughness of the films. The morphology and microstructure of the films was examined with a high resolution SEM (Edax Phoenix System, Edax Inc., Mahwah, NJ). The film thickness was also determined by SEM. In this case, a cross section of the single crystal coated with the film was mounted in epoxy resin and observed in the SEM.

3. Results

The reactant concentration employed in earlier work [20] for the homogeneous precipitation of $BaTiO_3$ particles from solution did not lead to the deposition of a film on the single crystal substrate. By reducing the reactant concentration at a fixed reaction temperature (150°C), film formation was eventually achieved. Film deposition is also sensitive to the presence of surface

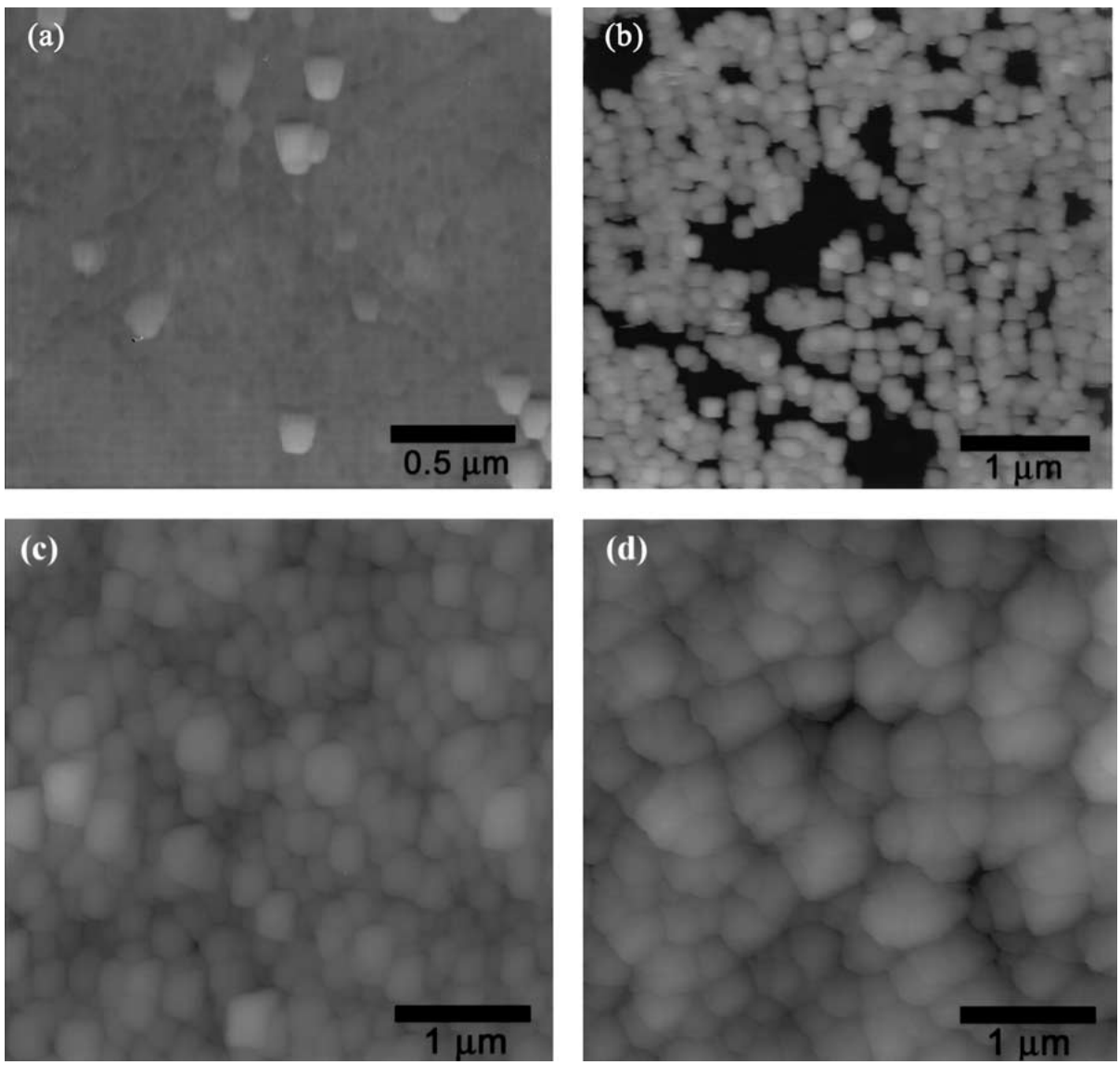

Figure 1 Atomic force microscopy images of $BaTiO_3$ films deposited on $SrTiO_3$ single crystal after reaction times of (a) 20 min, (b) 30 min, (c) 3 h, and (d) 9 h.

flaws on the substrate. The presence of scratches and other flaws on the substrate greatly hinder the formation of nuclei and, hence, the deposition of the film. Suspending the substrate in the reactant solution produced a more uniform film when compared to placing it at the bottom of the reaction vessel. Deposition of free $BaTiO_3$ particles on to the substrate hindered the deposition of the film when the substrate was situated at the bottom of the vessel.

Fig. 1 shows AFM images of the nucleation and growth of a $BaTiO_3$ film on a $SrTiO_3$ single crystal. The formation of nuclei was observed after $\sim$20 min at the reaction temperature (Fig. 1a) and this process proceeded rapidly, so that in another 10 min (total reaction time = 30 min), a considerable fraction of the substrate surface was covered (Fig. 1b). A remarkable feature is the almost uniform size and the almost cubic uniformity of the crystals (Fig. 1b), which may indicate a

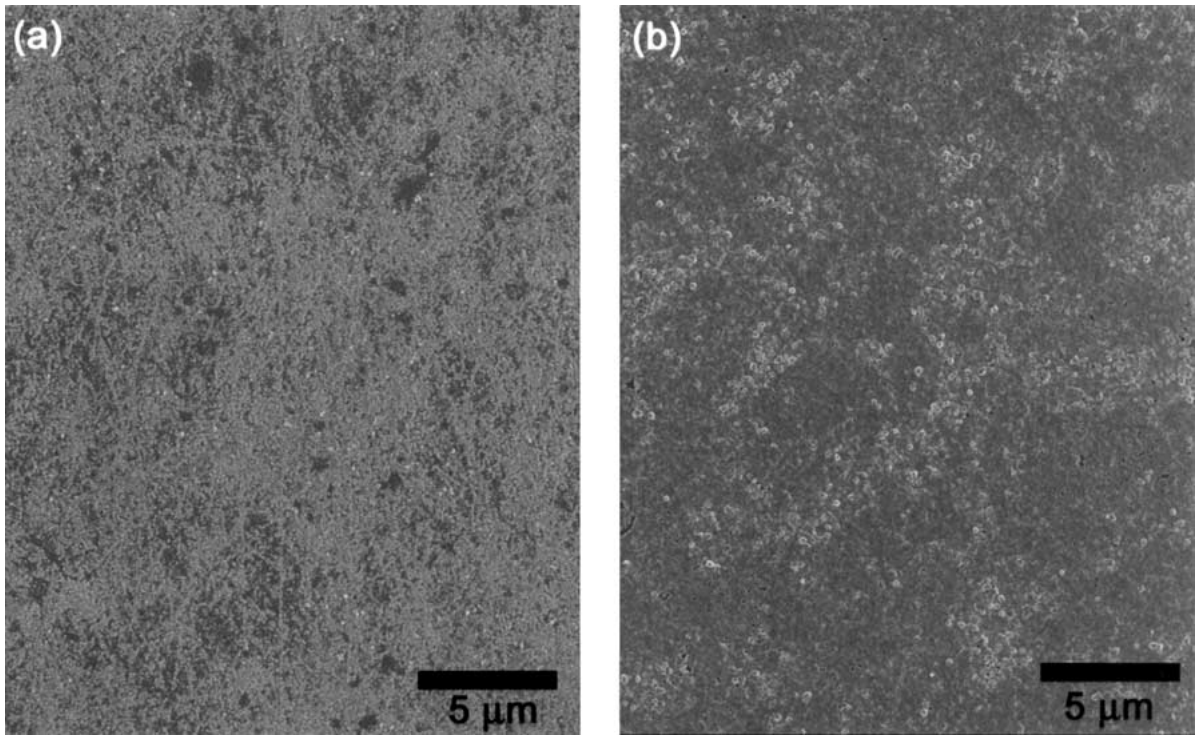

Figure 2 Scanning electron micrographs of $BaTiO_3$ film deposited on $SrTiO_3$ single crystal after reaction times of (a) 3 h, and (b) four cycles of 3 h each.

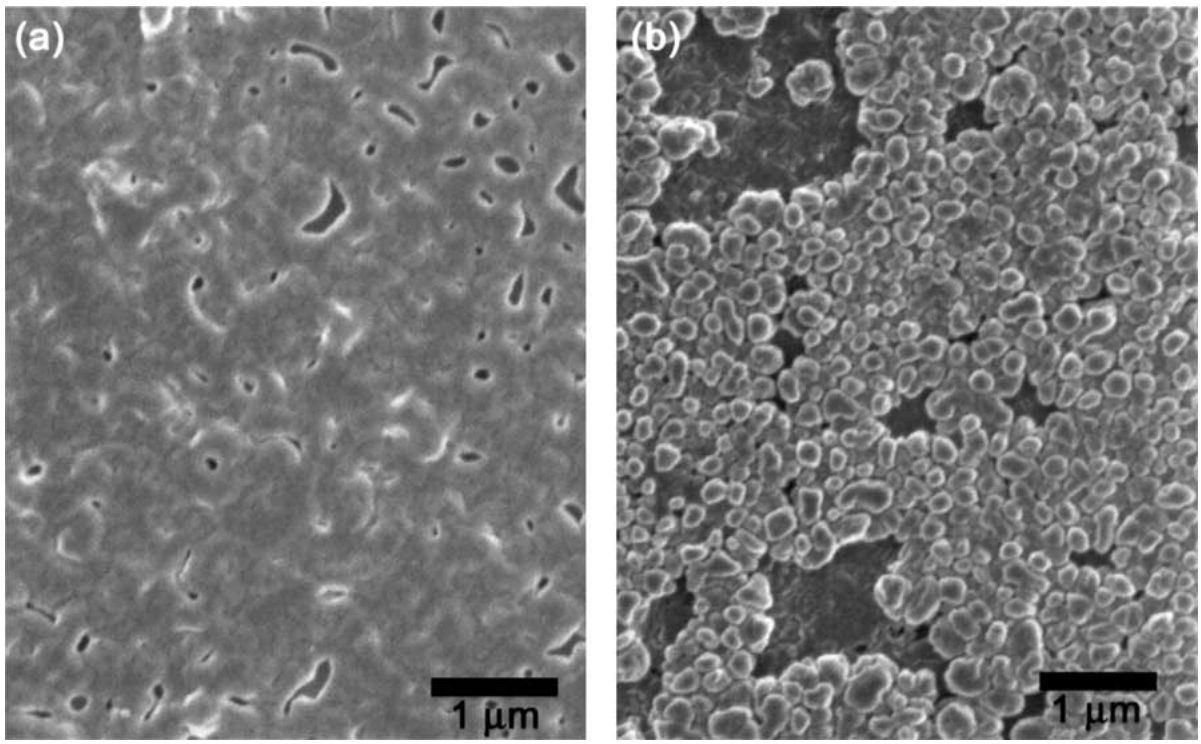

Figure 3 Scanning electron micrographs of $BaTiO_3$ films deposited on (a) $BaTiO_3$ single crystal and (b) $LaAlO_3$ single crystal for the same reaction conditions (4 cycles of 3 h each).

burst of nucleation within a narrow time frame. Further nucleation and three-dimensional growth of the crystals produced almost complete coverage of the substrate after 1.5 h (Fig. 1c). At longer reaction times, coarsening of the crystals and thickening of the film occur by the same nucleation and growth mechanism (Fig. 1d).

Fig. 2 shows SEM micrographs of the film deposited on $SrTiO_3$ after 3 h and after four cycles lasting 3 h each. The reactants were replaced after each cycle. After 3 h of deposition (Fig. 2a), the underlying scratches originally present on the substrate are still apparent due to their influence on the morphology of the deposited film. However, further nucleation and growth produces a dense film with a relatively smooth surface (Fig. 2b). High resolution SEM indicates the presence of some fine, isolated pores (Fig. 3a). An SEM micrograph of the film deposited on $LaAlO_3$ under the same conditions as those for the $SrTiO_3$ substrate is shown in Fig. 3b. The film is not as uniform as that deposited on $SrTiO_3$.

While AFM revealed almost complete coverage of the $SrTiO_3$ substrate by the film after ~1.5 h of reaction, the film became thick enough to produce measurable X-ray diffraction peaks after ~5 h of reaction. Fig. 4 shows XRD patterns acquired in the step-scan mode

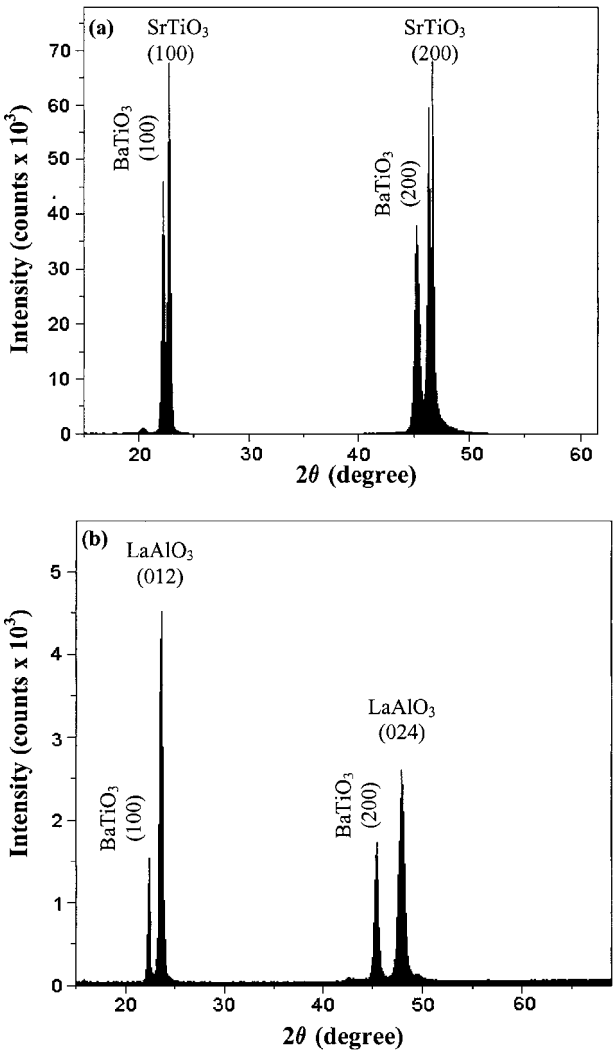

Figure 4 X-ray diffraction patterns of $BaTiO_3$ films deposited on (a) $SrTiO_3$ single crystal and (b) $LaAlO_3$ single crystal, showing that the films have the same out-of-plane orientation as the single crystal substrates.

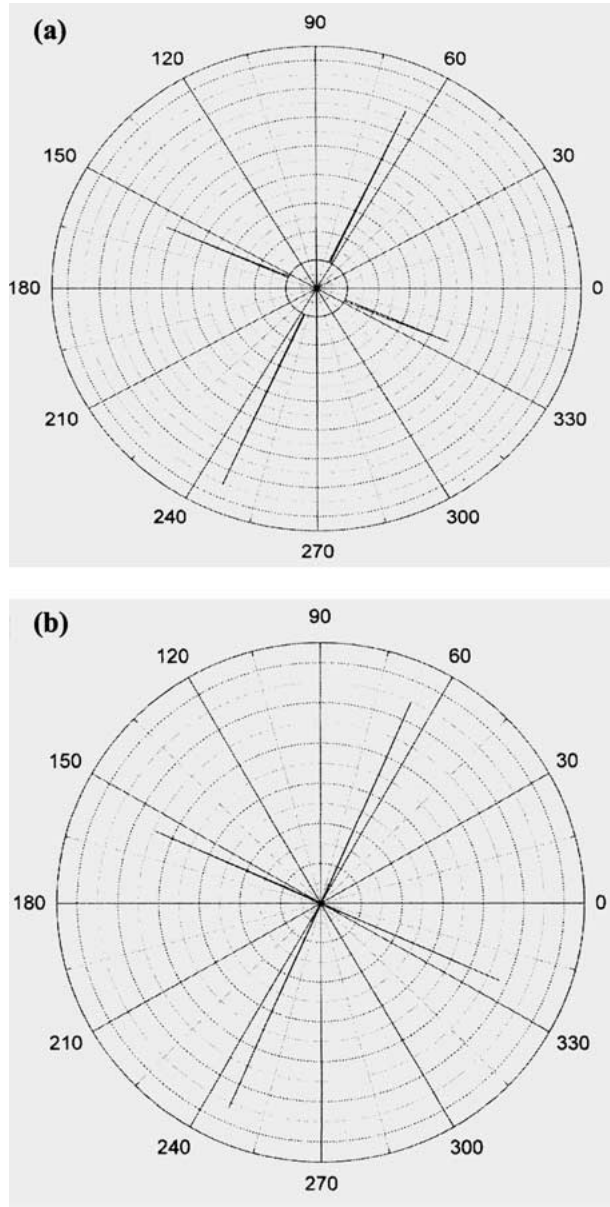

Figure 5 X-ray azimuthal scans (pole figures) for the (100) reflections of (a) $BaTiO_3$ film on $SrTiO_3$ single crystal and (b) uncoated $SrTiO_3$ single crystal, showing that the film has the same in-plane orientation as the single crystal substrate.

for films deposited on $SrTiO_3$ and $LaAlO_3$ after five cycles of reaction lasting 3 h each. Only the (100) and (200) reflections of the films are observed, indicating that the films have the same out-of-plane orientation as the substrates. X-ray azimuthal scans (pole figures) for the $BaTiO_3$ films deposited on $SrTiO_3$ and $LaAlO_3$ substrates and those for the corresponding substrate are shown in Figs 5 and 6. The pole figures indicate that the films have the same in-plane orientation as the substrate. The in-plane and out-of-plane orientation data indicate that the films are epitaxial in nature.

X-ray rocking curves for the (100) reflections of the films deposited on $SrTiO_3$ and $LaAlO_3$ are shown in Fig. 7. The full width at half maximum (FWHM) for the films and the substrates were measured and compared. The measured values are summarized Table I. Commonly, the FWHM for a polycrystalline material with a random arrangement of the crystals is ~10°. For single crystals, it is commonly <1°. The present

TABLE I Data for the full width at half maximum (FWHM) for the $BaTiO_3$ film and for the $SrTiO_3$ and $LaAlO_3$ single crystal substrates measured from the X-ray rocking curves for the (100) reflection

Material	FWHM (degrees)
$BaTiO_3$ film on $SrTiO_3$	0.38
$SrTiO_3$ single crystal	0.26
$BaTiO_3$ film on $LaAlO_3$	0.93
$LaAlO_3$ single crystal	0.65

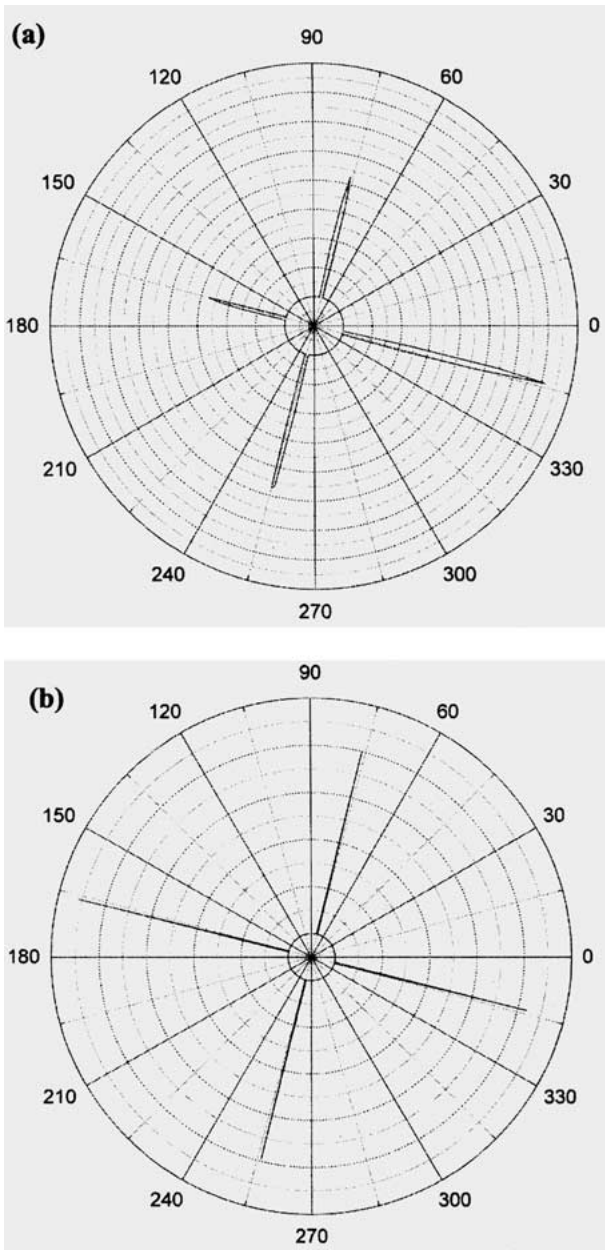

Figure 6 X-ray azimuthal scans (pole figures) for the (100) reflections of (a) $BaTiO_3$ film on $LaAlO_3$ single crystal and (b) uncoated $LaAlO_3$ single crystal, showing that the film has the same in-plane orientation as the single crystal substrate.

data indicate that while the FWHM values for the films are larger than the values for the single crystal substrates, they are less than 1°. These small values for the films can be taken as an indication of their good crystalline quality and high degree of alignment with the substrate.

SEM micrographs of the cross section of films deposited on $SrTiO_3$ showed that that the film thickness

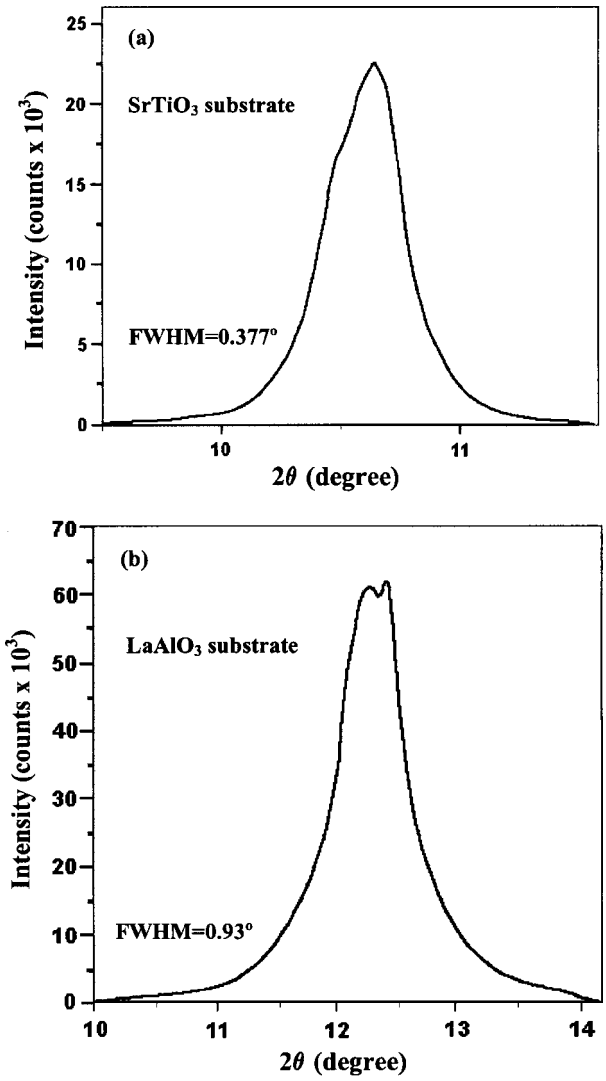

Figure 7 X-ray rocking curves for the (100) reflections of $BaTiO_3$ films deposited on (a) $SrTiO_3$ single crystal and (b) $LaAlO_3$ single crystal.

was ~150 nm after 1.5 h of deposition, at which time the substrate was almost fully covered. Further deposition produced a film thickness of ~600 nm after 5 cycles of reaction lasting 3 h each. Information on the surface roughness of the films was acquired by AFM. Fig. 8 shows quasi-three-dimensional images of the substrate surface and the film surface for films deposited after reaction times of 1.5 h, 9 h, and five repeated cycles of 3 h each. The roughness of the film appears to increase with deposition time but is not more than 150–200 nm.

4. Discussion

In the present experiments, the reactants consist of fine TiO_2 particles in a strongly alkaline solution of $Ba(OH)_2$. These conditions are consistent with thermodynamic predictions for the Ti-Ba-H_2O system [21] which indicate that $BaTiO_3$ is the thermodynamically favored phase at pH values greater then 12 and for high Ba^{2+} concentration (2 molar). Similar reaction conditions were also employed for the synthesis of $BaTiO_3$ particles [16, 20] and epitaxial thin films [16–19]. Based on these studies, the thermodynamic foundation for the synthesis of $BaTiO_3$ appears well established.

The reaction mechanism is not clear but it has been suggested to involve a dissolution/precipitation process

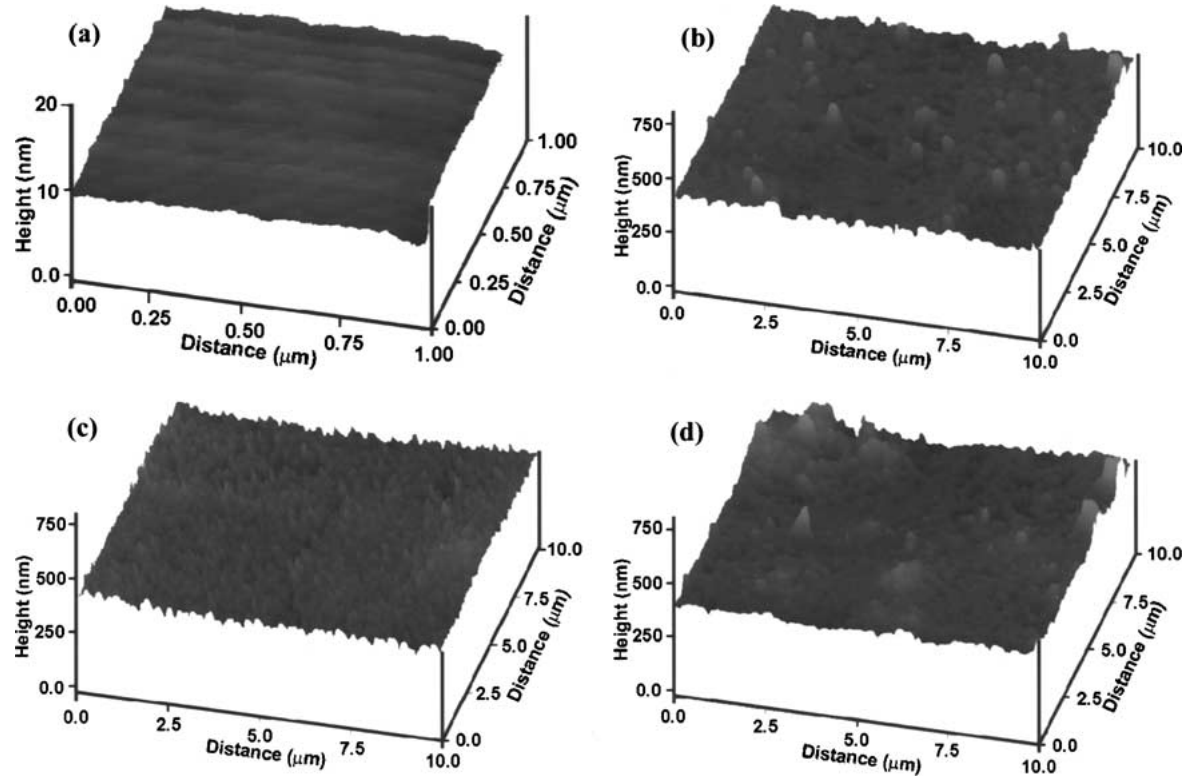

Figure 8 Atomic force microscopy images of (a) the surface of an uncoated $SrTiO_3$ single crystal, and the surfaces of $BaTiO_3$ films deposited on $SrTiO_3$ single crystals after reaction times of 1.5 h (b), 3 cycles of 3 h each (c), and five cycles of 3 h each (d).

in which Ti is hydrolyzed to form either $Ti(OH)_6^{2-}$ [9] or $Ti(OH)_4$ [13] followed by subsequent reaction with Ba^{2+} to precipitate $BaTiO_3$. In the present reaction system, several interactions are possible. The $BaTiO_3$ can nucleate homogeneously in solution and grow to form particles (or agglomerates), leading to an uncoated substrate and a precipitate of fine particles. Nucleation can also occur heterogeneously on the fine TiO_2 reactant particles, resulting again in an uncoated substrate and fine $BaTiO_3$ particles. As outlined earlier, the reactant concentrations used in earlier work [20] to synthesize $BaTiO_3$ particles did not lead to film deposition. By reducing the concentration of the reactants at a fixed reaction temperature (150°C), film deposition was eventually achieved. The concentration of the reactants is therefore a key variable in the deposition process.

The deposition of the film is also dependent on the surface finish and crystal structure of the single crystal substrate. As outlined earlier, the formation of nuclei was inhibited by the presence scratches and other flaws on the surface of the substrate. The lattice mismatch between the film and the substrate is also a key parameter. The lattice mismatch is defined as:

$$\varepsilon = (a_f - a_s)/a_s \quad (1)$$

where a_s and a_f are the lattice parameters of the substrate and the film, respectively. For the film and substrate materials investigated in the present work, the lattice parameters and lattice mismatch values are given in Table II. Two important issues are first, the influence of the magnitude of the lattice mismatch on the ability to deposit a film by hydrothermal precipitation and second, the mechanism by which the lattice mismatch

TABLE II Lattice parameter and lattice mismatch values for the $BaTiO_3$ film and the $SrTiO_3$ and $LaAlO_3$ single crystal substrates

Material	Lattice constant (nm)	Lattice mismatch strain
Film		
$BaTiO_3$ (cubic)	0.4031	–
Substrate		
$SrTiO_3$ (cubic)	0.3905	+0.032
$LaAlO_3$ (pseudocubic)	0.3790	+0.064

is accommodated at the interface between the film and the substrate. The present data indicate that a mismatch value of 6.4% (for the film on the $LaAlO_3$ substrate) is not high enough to inhibit the deposition of the epitaxial $BaTiO_3$ film. However, a comparison of Fig. 3a and b appears to indicate that the film on the $LaAlO_3$ substrate is less uniform microstructurally when compared to the film on the $SrTiO_3$ substrate (lattice mismatch = 3.2%). For epitaxial films deposited on single crystal substrates by electrochemical methods [4], lattice mismatch values as high as ~40% have been accommodated. Further experiments using substrates with higher mismatch values than those used in the present experiments are required to clarify the effect of lattice mismatch on the ability to deposit epitaxial films under hydrothermal conditions.

The accommodation of the lattice mismatch at the interface between the film and the substrate was not investigated in the present work. However, TEM studies by Chien *et al.* [18] indicate that the mismatch between the $BaTiO_3$ film and the $SrTiO_3$ substrate is accommodated by misfit dislocations with a periodicity of ~11 nm, which coincides with the calculated

periodicity of ~12 nm for misfit dislocations based on the 3.2% mismatch between cubic $BaTiO_3$ and $SrTiO_3$. TEM studies by Langjahr *et al*. [22] on epitaxial perovskite films prepared on perovskite substrates by solution-based methods also reveal that the lattice mismatch in these systems is accommodated by dislocations. For electrochemically deposited films on substrates with much higher lattice mismatch, Switzer *et al*. [4] observed that the film lattice is rotated relative to that of the substrate.

The AFM images (Fig. 1) coupled with the XRD data indicate that film deposition occurs by nucleation of {001} faceted islands followed by three-dimensional growth of the islands to cover the substrate. A similar nucleation and growth mechanism was observed by Chien *et al*. [18] for $BaTiO_3$ films deposited on $SrTiO_3$ at lower synthesis temperatures (90°C). Although a detailed investigation was not performed in the present work, the AFM and SEM images appear to indicate that after coverage of the substrate by the first $BaTiO_3$ layer, thickening of the film occurs by sequential deposition of additional layers by the same island growth mechanism. If the film had thickened rapidly relative to the coverage of the substrate, then a very rough surface with perhaps regions of uncovered substrate would have resulted, which is not seen (Fig. 8).

5. Conclusions

Relatively dense heteroepitaxial $BaTiO_3$ thin films with a thickness in the range of 150 to 600 nm were deposited on single crystal substrates of (100) $SrTiO_3$ and (012) $LaAlO_3$ by reacting fine TiO_2 particles in a strongly alkaline solution of $Ba(OH)_2$ under hydrothermal conditions at 150°C. The formation of the films occurred by nucleation of {100} faceted islands followed by three-dimensional growth of the islands to produce nearly complete coverage of the substrate in ~1.5 h. The thickening of the film occurred by the sequential deposition of additional layers by the same island growth mechanism. The films had a high quality of crystallinity as reflected by the narrow width of the X-ray rocking curves, and the same in-plane and out-of-plane orientation as the substrate.

Acknowledgements

The authors would like to thank Dr. J. A. Switzer for use of AFM facilities and Y. Rue for assistance with the AFM observations.

References

1. R. E. NEWNHAM, *Rep. Prog. Phys*. **52** (1989) 123.
2. R. G. DOSCH, *Mater. Res. Soc. Symp. Proc*. **32** (1984) 157.
3. B. W. WESSELS, *Ann. Rev. Mater. Sci*. **25** (1995) 525.
4. E. BOHANNON, M. G. SHUMSKY and J. A. SWITZER, *Chem. Mater*. **11** (1999) 2289.
5. W.-S. HO, M. YASHIMA, M. KAKIHANA, A. KUDO, T. SAKATA and M. YOSHIMURA, *J. Amer. Ceram. Soc*. **78** (1995) 3110.
6. P. BENDALE, S. VENIGALLA, J. R. AMBROSE and E. VERINK, JR., *ibid*. **76** (1993) 2619.
7. W. J. DAWSON, *Amer. Ceram. Soc. Bull*. **67** (1988) 1673.
8. M. YOSHIMURA and W. SUCHANEK, *Solid State Ionics* **98** (1997) 197.
9. M. YOSHIMURA, S. E. YOO, M. HAYASHI and N. ISHIZAWA, *Jpn. J. Appl. Phys*. **28** (1989) 2007.
10. Q. CHEN, Y. QIAN, Z. CHEN, W. WU, Z. CHEN, G. ZHOU and Y. ZHANG, *Appl. Phys. Lett*. **66** (1995) 1608.
11. Q. CHEN, Y. QIAN, Z. CHEN, G. ZHOU and Y. ZHANG, *Mater. Lett*. **22** (1995) 93.
12. K. KAJIYOSHI, N. ISHIZAWA and M. YOSHIMURA, *J. Amer. Ceram. Soc*. **74** (1991) 369.
13. R. BACSA, P. RAVINDRANATHAN and J. P. DOUGHERTY, *J. Mater. Res*. **7** (1992) 423.
14. R. R. BACSA, J. P. DOUGHERTY and L. J. PILLONE, *Appl. Phys. Lett*. **63** (1993) 1053.
15. K. KAJIYOSHI, N. ISHIZAWA and M. YOSHIMURA, *Jpn. J. Appl. Phys*. **30** (1991) L120.
16. A. T. CHIEN, J. S. SPECK, F. F. LANGE, A. C. DAYKIN and C. G. LEVI, *J. Mater. Res*. **10** (1995) 1784.
17. A. T. CHIEN, J. S. SPECK and F. F. LANGE, *ibid*. **12** (1997) 1176.
18. A. T. CHIEN, L. ZHAO, M. COLIC, J. S. SPECK and F. F. LANGE, *ibid*. **13** (1998) 649.
19. A. T. CHIEN, X. XU, J. H. KIM, J. SACHLEBEN, J. S. SPECK and F. F. LANGE, *ibid*. **14** (1999) 3331.
20. E. CIFTCI, M. N. RAHAMAN and M. G. SHUMSKY, *J. Mater. Sci*. **36** (2001) 4875.
21. K. OSSEO-ASARE, F. J. ARRIAGADA and J. H. ADAIR, *Ceramic Trans*. **1** (1988) 47.
22. P. A. LANGJAHR, F. F. LANGE, T. WAGNER and M. RÜHLE, *Acta Mater*. **46** (1998) 773.

Received 5 December 2001
and accepted 23 April 2002